ARTICLE

Rh Promoted In_2O_3 as Highly Active Catalyst for CO_2 Hydrogenation to Methanol

Received 00th January 20xx,
Accepted 00th January 20xx

DOI: 10.1039/x0xx00000x

Nazmul Hasan MD Dostagir,[a,b] Coogan Thompson,[c] Hirokazu Kobayashi,[a] Ayman M. Karim,[c] Atsushi Fukuoka*[a] and Abhijit Shrotri*[a]

Synthesis of methanol with high selectivity and productivity through hydrogenation of CO_2 is highly attractive. This work uses Rh doped In_2O_3 catalyst to achieve high methanol productivity of 1.0 g_{MeOH} h^{-1} g_{cat}^{-1} while maintaining the intrinsic high selectivity of pure In_2O_3. Rh facilitated the dissociation of H_2 leading to creation of oxygen vacancy over the In_2O_3 surface. In addition, Rh atoms also participated in activation of CO_2 to produce formate species with a low activation barrier as evidence by DFT calculation. Rh species were atomically dispersed in the In_2O_3 matrix and were stable during long term reaction. Under reaction condition the surface Rh atoms were reduced and were stabilized by charge transfer from neighbouring In atoms. Our results show that incorporation of atomic Rh species in In_2O_3 can lead to high methanol productivity by creation of oxygen vacancy as well as Rh centred active sites for CO_2 activation.

Introduction

Synthesis of methanol by direct catalytic hydrogenation of CO_2 is attractive because methanol is produced in large volumes and finds application as a fuel, solvent and precursor for bulk chemicals.[1] Catalyst design to improve methanol selectivity and productivity at high CO_2 concentrations is a challenge in development of this process. The endothermic reverse water-gas shift (rWGS) reaction (equation 1) competes with the exothermic methanol formation (equation 2) in a CO_2 rich feed.[1]

$$CO_2 + H_2 \Leftrightarrow CO + H_2O \qquad \Delta H^{\circ}_{298K} = +41.2\ kJ\ mol^{-1} \quad (1)$$

$$CO_2 + 3H_2 \Leftrightarrow CH_3OH + H_2O \quad \Delta H^{\circ}_{298K} = -49.5\ kJ\ mol^{-1} \quad (2)$$

The industrial catalyst, Cu-ZnO/Al_2O_3, deactivates rapidly in the presence of a CO_2 rich feedstock.[2] In the quest of a selective and stable catalyst for CO_2 hydrogenation to methanol, In_2O_3 has emerged as an attractive alternative. In_2O_3 with oxygen vacancy can suppress RWGS reaction to produce methanol with high selectivity and is stable at high CO_2 concentration.[3] Oxygen vacancy along with neighboring In atom can dissociate hydrogen heterolytically and perform CO_2 hydrogenation. Methanol selectivity of 100% can be achieved over pure In_2O_3 catalyst at low temperature, however, the space-time yield (STY) of methanol remains low owing to low CO_2 conversion over pure In_2O_3.[4] Several promotional strategies were applied to improve the activity, albeit the methanol productivity remained low. The CO_2 conversion and catalyst stability was improved by supporting In_2O_3 over on ZrO_2.[4] Electronic interaction with ZrO_2 promoted the generation of oxygen vacancies over In_2O_3 surface and reduced sintering. The interface of Cu_2In species with In_2O_3 also improved the generation of oxygen vacancies and improved methanol productivity.[5] Charge transfer from Co support to In_2O_3 film also led to creation of oxygen vacancies in an In@Co catalyst resulting in methanol productivity of 0.86 g_{MeOH} h^{-1} g_{cat}^{-1}.[6]

Addition of noble transition metals resulted in high methanol productivity. Theoretical analysis predicted that, in the presence of Pd_4 clusters, dissociation and spillover of H_2 over In_2O_3 surface was enhanced.[7] Rui et al. experimentally showed that In_2O_3 supported Pd catalyst having small Pd particles, without producing Pd-In alloy, achieved a methanol productivity of 0.89 g_{MeOH} h^{-1} g_{cat}^{-1}.[8] Snider et al. reported that a synergy between In_2O_3 and In_3Pd_2 intermetallic compound in a In-Pd/SiO_2 catalyst was crucial for the promotional effect.[9] Recently, low-nuclearity clusters of In with transition metals such as Pd[10] and Rh[11] were shown to be effective for high methanol productivity. $Pd_2In_2O_4$ and $Pd_3In_2O_4$ clusters were suggested as the active sites for the high selectivity of methanol and Pd clusters with a nuclearity higher than 4 caused increase in CO selectivity.[10] Li et al. suggested that formation of bimetallic RhIn nanoparticles were helpful to achieve high methanol productivity (1.0 g_{MeOH} h^{-1} g_{cat}^{-1}).[11] Decoration of reduced In over Rh nanoparticles forming bimetallic RhIn and $RhIn_3$ alloy nanoparticles of 1-3 nm helps in the formation of formate species (intermediate for methanol) as compared to carboxyl species (intermediate for CO).

From the above discussion, it is evident that while the formation of oxygen vacancy and hydrogen dissociation are enhanced in the presence of metals, they have additional influence on the catalytic activity of In_2O_3. Although several

[a] Institute for Catalysis, Hokkaido University, Kita 21 Nishi 10, Kita-ku, Sapporo, Hokkaido 001-0021, Japan. E-mail: ashrotri@cat.hokudai.ac.jp, fukuoka@cat.hokudai.ac.jp.
[b] Graduate School for Chemical Sciences and Engineering, Hokkaido University Kita 13 Nishi 8, Kita-ku, Sapporo, Hokkaido 060-8628, Japan.
[c] Department of Chemical Engineering, Virginia Polytechnic Institute and State University, Blacksburg, Virginia 24060, United States.
†Electronic Supplementary Information (ESI) available: See DOI: 10.1039/x0xx00000x

promotional strategies were employed, there is little knowledge about the effect of dopant in In_2O_3 for CO_2 hydrogenation to methanol. Therefore, we designed In_2O_3 catalysts doped with transition metals from group 8, 9 and 10 of the periodic table to find out the best promotor for In_2O_3 and investigate the influence of atomically dispersed promotors on catalytic activity. The dopants of these groups are known to have high H_2 dissociation ability which would facilitate the hydrogenation reaction. Although metals in these groups tend to sinter when interaction with the support is weak, In_2O_3 being a reducible support can stabilize the dopants. Our results show that atomically dispersed Rh is highly effective for this reaction and it activates and hydrogenates CO_2 apart from creating oxygen vacancy on the surface and helping in H_2 dissociation.

Experimental

Catalyst Preparation. In_2O_3 mix-oxide catalyst was prepared by using sol-gel method in the presence of citric acid. A typical procedure to obtain Rh-1.3-In_2O_3 catalyst is as follows. $In(NO_3)_3{\cdot}3H_2O$ (4.75 mmol) and $Rh(NO_3)_3$ (0.062 mmol) were added to a beaker containing 30 mL of distilled water along with 5 mmol of citric acid. The beaker was placed over a hot plate maintained at 130 °C and stirred until a foaming gel was formed. The gel was then dried by placing the beaker in an oven maintained at 130 °C for 5 h. The resulting composite was crushed and calcined to obtain the final catalyst. Other catalysts were prepared by changing the amount or type of the second metal precursor. Catalysts were named as M-X-In_2O_3, where X is the atom% of M with respect to total metal content (M + In) of the catalyst and M represents the type of dopant metal (Fe, Ru, Co, Rh, Ni, Pd, or Pt). Undoped In_2O_3 was produced using the same method in the absence of dopant precursors. Rh-1.3-ZnO was also prepared using this method by replacing $In(NO_3)_3{\cdot}3H_2O$ with $Zn(NO_3)_2{\cdot}6H_2O$.

For comparison, catalyst was made using co-precipitation and wet impregnation method (supporting information).

All catalysts were calcined at 500 °C for 3 h (ramp rate = 2 °C min^{-1}).

Catalyst characterization. Temperature programmed reduction (TPR) of catalysts were carried out in presence of H_2-Ar mixture (H_2 = 5%) in a BELCAT II instrument equipped with a TCD detector. Prior to measurement, catalysts were pretreated at 150 °C for 1 hour under Ar flow. Measurements were done at a total flow rate of 50 mL min^{-1} with ramp rate of 10 °C min^{-1}. CO Pulse chemisorption was also performed in the BELCAT II at 50 °C. Prior to the measurement, samples were reduced under H_2 flow at 200 °C for 1h. Calculations were done considering the stoichiometric ratio of Rh:CO = 1:2 because Rh single atom binds with two CO molecule.[12] CO_2 TPD experiment was performed in the BELCAT II instrument equipped with BELMass gas mass spectrometer. Prior to measurement, the samples were pretreated either with Ar or with a mixture of CO_2:H_2 (1:4) at 300 °C for 30 min. The sample was then cooled to room temperature under gas flow and then He was used to purge the sample sell for 30 min. In TPD analysis under He flow, temperature was increased by 10 °C min^{-1}. For formic acid TPD, formic acid was first impregnated on the catalyst in a hexane solution. The impregnated catalyst was washed with hexane to remove the physisorbed formic acid and was dried at room temperature. The TPD analysis was carried out under He flow and temperature was increased by 10 °C min^{-1}. CO DRIFTS over Rh-1.3-ZnO were recorded in a Perkin Elmer Spectrum 100 FTIR spectrometer equipped with MCT detector cooled with liquid N_2 using Kubelka Munk approximation. The catalyst was reduced at 200 °C for 1 h under H_2 flow, then cooled to 25 °C under He flow. The background spectrum was recorded at this condition. 1.17% CO/He mixture gas was introduced thereafter. Spectrum consisting of both gaseous and adsorbed CO was recorded in this condition. After 10 min, pure He flow was started to flow and kept for 15 min to eliminate gaseous CO. Data for adsorbed CO species was recorded in this condition.

XAS measurements at the Rh K-edge of the Rh-1.3-In_2O_3 (fresh and used) and $Rh(acac)_3$ samples were performed at the Stanford Synchrotron Radiation Light Source (SSRL) at beamline 4-1. This beamline is an unfocused, 20-pole, 2-Tesla wiggler side station with a vertical collimating mirror. The samples were prepared via pressing 70 mg of the catalyst into a pellet approximately 7 mm in diameter. The pellet was then placed between two layers of Kapton tape and held in the beam line at a 45-degree angle in the direction of the fluorescence Lytle detector. XAS data was collected from 22984 to 24081 eV (~ 14.9 1/Å in k-space) on both the sample and a Rh metal reference foil simultaneously. In order to improve the signal to noise ratio, four scans (11 minutes each) were collected, then aligned and merged using the Rh foil spectrum collected simultaneously for each scan. Samples were scanned simultaneously in transmission and fluorescence detection modes using ion chambers (filled with argon) and the Lytle detector, respectively.

Evaluation of catalytic activity. Catalytic activity for CO_2 hydrogenation was evaluated in a stainless-steel packed bed flow system (Figure S1). Products were analysed using an online GC (Shimadzu, GC 8A) equipped with two columns – Porapak Q and Molecular Sieve and a TCD detector. Gas line from the outlet of the reactor to the inlet of the GC was heated at 150 °C to prevent condensation of methanol and H_2O. Typically, 200 mg of catalyst (mixed with equal amount of silicon carbide (SiC) was loaded into the reactor and held in place by quartz wool. A thermocouple was inserted into the reactor to measure catalyst bed temperature. Prior to reaction, the catalyst was pretreated under 0.5 MPa Ar for 1 h at 300 °C. Then the reactor was cooled to 50 °C under Ar and pressurized to reaction condition using a mixture of H_2, CO_2 and Ar having the ratio H_2:CO_2:Ar = 4:1:1. After the system pressure was stable, reactor temperature was increased to desired value. Reactions at space velocity (SV) higher than 30,000 mL h^{-1} g^{-1} were carried out by lowering the amount of catalyst and maintaining the same gas flow rate.

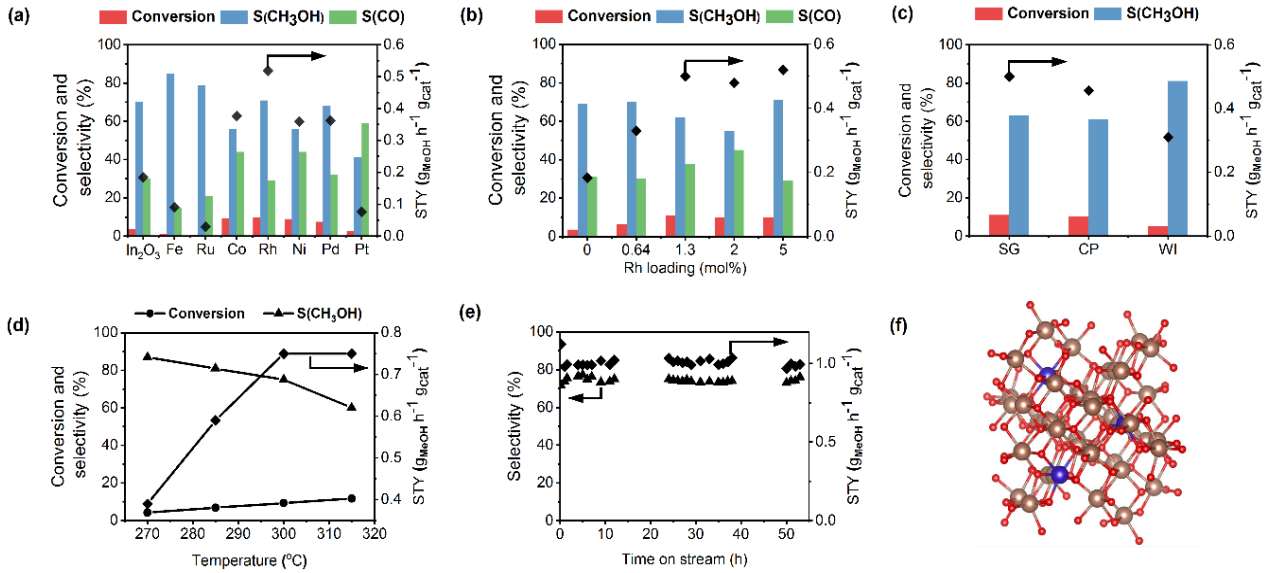

Fig. 1. (a) Screening of different metal promoters (reaction condition: M-5-In_2O_3, 270 °C, 5 MPa, 30,000 mL h^{-1} g_{cat}^{-1}, H_2/CO_2 = 4), (b) optimization of Rh loading (reaction condition: Rh-X-In_2O_3, 270 °C, 5 MPa, 30,000 mL h^{-1} g_{cat}^{-1}, H_2/CO_2 = 4), (c) comparison of Rh-1.3-In_2O_3 catalysts prepared using different methods. SG, CP and WI represent sol-gel, co-precipiatation and wet impregnation methods respectively (reaction condition: 270 °C, 5 MPa, 30,000 mL h^{-1} g_{cat}^{-1}, H_2/CO_2 = 4). (d) effect of temperature on methanol production from CO_2 (reaction condition: Rh-1.3-In_2O_3, 5 MPa, 45,000 mL h^{-1} g_{cat}^{-1}, H_2/CO_2 = 4), (e) evaluation of methanol selectivity and STY over time of stream (reaction condition: Rh-1.3-In_2O_3, 300 °C, 5 MPa, 60,000 mL h^{-1} g_{cat}^{-1}, H_2/CO_2 = 4), (f) graphical representation of Rh doped into In_2O_3 (110) plane (blue for Rh, brown for In and red for oxygen atom respectively).

Results and discussion

When used for CO_2 hydrogenation, pure In_2O_3 produced methanol (STY = 0.18 g_{MeOH} h^{-1} g_{cat}^{-1}) with a selectivity of 70% and CO_2 conversion of 3.7% at 270 °C, 5 MPa pressure and 30,000 mL h^{-1} g_{cat}^{-1} of space velocity (SV) (Fig. 1a). Addition of Fe, Ru, and Pt as dopants did not have a favourable promotional effect. Fe and Ru doped catalysts produced methanol with 87% and 79% selectivity respectively. However, the CO_2 conversion was low resulting in low STY. Pt doped catalyst produced CO as the major product and methanol selectivity was only 41%. Doping of Pd, Rh, Ni, and Co improved the methanol yield. Pd doped catalyst produced methanol with similar selectivity to In_2O_3 (68%) with increased CO_2 conversion (7.5%). Pd-5-In_2O_3 promoted methanol STY to 0.36 g_{MeOH} h^{-1} g_{cat}^{-1}, 2 times higher than that over pure In_2O_3. Productivity of methanol over catalysts after doping of Co, Ni were similar to that of Pd albeit with a slightly lower selectivity. Ni and Co doped catalysts showed higher CO_2 conversion (9 and 9.4%) as compared to Pd promoted analog, although methanol selectivity was slightly lower (56%). These results show that the promotional effect of dopants is not restricted to their hydrogen dissociation ability. Rh promoted In_2O_3 (Rh-5-In_2O_3) outperformed others with a high CO_2 conversion of 10% while maintaining a selectivity of 71% producing methanol with 2.9 times higher STY (0.52 g_{MeOH} h^{-1} g_{cat}^{-1}) than pure In_2O_3.

Rh loading of 5 atom% (based on total metal content) was not vital for promotional effect and the catalytic activity was maintained until the Rh loading was as low as 1.3 atom% (equivalent to 0.96 wt.%, Fig. 1b). Even lower Rh loading of 0.64 atom% also showed promotional effect with an STY of 0.33 g_{MeOH} h^{-1} g_{cat}^{-1} which was 1.8 times higher than that for pure In_2O_3. Further experiments were done using Rh-1.3-In_2O_3. Catalyst synthesis procedure also influenced the activity and selectivity. Rh inclusion using sol-gel method was compared with co-precipitation and impregnation methods (Fig. 1c). Sol-gel catalyst performed better than the co-precipitation catalyst which outperformed catalyst prepared by impregnation. Higher surface concentration of Rh atoms in the sol-gel catalyst was the reason for its better activity (*vide infra*).

Increasing the space velocity had a positive influence on the selectivity of methanol. When the SV was increased from 30,000 to 45,000 mL h^{-1} g_{cat}^{-1} at 270 °C, methanol selectivity increased from 71% to 87%. However, due to lower contact time, the STY reduced to 0.39 g_{MeOH} h^{-1} g_{cat}^{-1} owing to lower CO_2 conversion (4.2%) (Figure 1d). Increase in reaction temperature had a favourable effect over STY till 300 °C and the conversion increased from 4.2% to 9.3% with a selectivity of 75% resulting an STY of 0.75 g_{MeOH} h^{-1} g_{cat}^{-1}. Further increase in temperature did not alter the methanol STY. Beyond 300 °C, methanol selectivity was reduced, and CO formation was promoted (Fig. 1d). In our study, the best result was obtained at 300 °C and 60,000 mL h^{-1} g_{cat}^{-1} SV resulting in STY of 1.0 g_{MeOH} h^{-1} g_{cat}^{-1} (Fig. 1e), one of the highest reported STY so far for In_2O_3 based catalysts. Further increase in the space velocity decreased the conversion. The catalyst was stable for more than 50 h of reaction without any loss of selectivity and maintained the STY of 1.0 g_{MeOH} h^{-1} g_{cat}^{-1} in the presence of Rh-1.3-In_2O_3 catalyst.

The Rh doped In_2O_3 catalysts were characterized thoroughly to understand the influence of Rh atoms on the structure. We used a sol-gel method with citric acid to produce mixed oxide catalyst in order to avoid inhomogeneity in metal distribution. Consequently, a fraction of Rh atoms were located on the surface and the rest were embedded within the In_2O_3 crystal. The amount of CO adsorbed over sol-gel catalyst (76 µL g^{-1}) indicated that 7.3% of Rh atoms were located on the surface. In comparison, the amount of CO adsorbed over co-precipitation

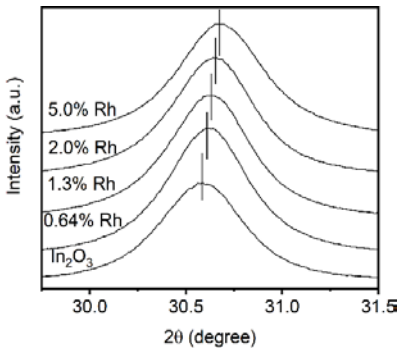

Fig. 2. Shifting of In_2O_3 (222) peak in XRD upon doping of Rh

catalyst (70 µL g^{-1}) and impregnation catalyst (48 µL g^{-1}) was lower, suggesting a lower surface concentration of Rh, which was in accordance with their catalytic activity. The surface ratio of Rh and In calculated from XPS also supported this observation. For sol-gel catalyst the observed Rh/In ratio from XPS was 0.018 in comparison to 0.012 for co-precipitation catalyst.

Surface area of Rh doped sol-gel catalysts varied only slightly in comparison to pure In_2O_3, which had a surface area of 27 m^2 g^{-1}. Incorporation of Rh introduced some porosity as evidence by the hysteresis loop in N_2 adsorption isotherm (Figure S2), which led to slight increase in surface area (41 m^2 g^{-1} for 1.3 Rh-In_2O_3). The change in surface area had no influence on catalytic activity as other dopants also caused a similar increase in the surface area without the promotional effects.

High-angle annular dark-field scanning transmission electron microscopy (HAADF-STEM) images of Rh-1.3-In_2O_3 (Fig. S3a-b, e-f) showed particles of In_2O_3 with size of 15-20 nm. Rh nanoparticles were not visible in fresh or used catalysts. Uniform distribution of Rh and In was observed in the EDX images (Fig. S3c-d, g-h; Fig. S4). However, Individual Rh atoms could not be identified in atomic resolution HAADF-STEM because Rh and In atoms appear with same brightness owing to their similar atomic numbers. Doping of Rh did not alter the structure (cubic) or size of In_2O_3 crystals (Fig. S5). Peaks for Rh_2O_3 were not observed in X-ray diffraction (XRD) analysis before or after the reaction (Fig. S6). However, the peak positions were shifted to higher 2θ values with increasing Rh loading (Fig. 2). This shifting was a result of reduction in interplanar spacing in In_2O_3 owing to the replacement of one In^{3+} ion with Rh^{3+} having smaller ionic radius (0.66 Å) than In^{3+} (0.8 Å).[13] A concurrent decrease in the value of lattice parameter was also observed with increasing Rh doping (Table S1). Therefore, we conclude that Rh was incorporated in the In_2O_3 crystal matrix forming a perfect mixed oxide at all loadings without the formation of Rh clusters.

The local chemical environment of Rh was probed using X-ray absorption fine structure (XAFS) analysis. The Rh absorption K-edge for fresh and used Rh-1.3-In_2O_3 catalysts was at a higher energy than metallic Rh. However, the absorption edge for Rh in the used catalyst was slightly lower than the fresh catalyst (Fig. 3a). The extended X-ray absorption fine structure (EXAFS) spectra (Fig. 3b) were fitted by replacing an In atom in the structure of cubic In_2O_3 with Rh (Table S2). The first Rh-O shell

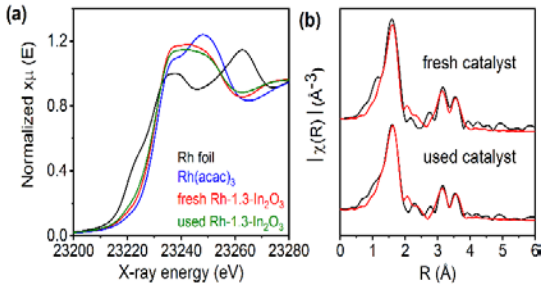

Fig. 3. (a) XANES and (b) EXAFS spectra of fresh and used Rh-1.3-In_2O_3 catalysts. Black and red lines in EXAFS spectra represent the data and model fit respectively.

had an expected coordination of 6.1 ± 0.7 for the fresh catalyst. The Rh-O bond length of 2.05±0.01 Å was lower than the expected In-O bond length due to lattice contraction supporting the XRD results.[14] Rh-In coordination distance in the second and the third shells at 3.30±0.01 and 3.82±0.03 Å were also slightly lower than that for In-In in pure In_2O_3.[15] This indicates the replacement of In atom with Rh atom in the crystal. For the used catalyst, the coordination number with oxygen reduced to 5.2±0.6. However, the coordination number for Rh-In shell was not altered. Lower co-ordination of Rh-O in the used catalyst could be due to reduction of surface Rh atoms during the reaction. Nevertheless, presence of Rh-Rh co-ordination was not observed in both the fresh and used catalysts (Fig. S7). These results along with XRD and HAADF-STEM indicate that Rh atoms are present as atomically dispersed species in the In_2O_3 matrix (Fig. 1f). Moreover, intermetallic RhIn and $RhIn_3$ type structures reported as active sites in co-precipitated Rh-In_2O_3/Al_2O_3 catalyst were not observed. [11]

X-ray photoelectron spectroscopy (XPS) analysis of Rh-1.3-In_2O_3 catalysts was used to elucidate state of surface and near surface Rh atoms (Fig. 4). In fresh Rh-1.3-In_2O_3, along with the prominent Rh $3d_{5/2}$ peak at 308.7 eV for Rh^{3+}, a small peak at 307.2 eV with the oxidation state close to 0 was also observed owing to the partial reduction of surface Rh species during XPS measurement.[16,17] The peak at 307.0 eV in the used catalyst indicates a $Rh^{\delta-}$ state of surface Rh atoms after the reaction (Fig. 4b).[12] Charge transfer from partially reduced neighboring In atoms would increase the electron density on Rh causing the shift of binding energy. The simultaneous formation of partially reduced In atoms was also observed in the MNN spectra of used Rh-1.3-In_2O_3 catalyst (Fig S8). A shoulder peak appeared at

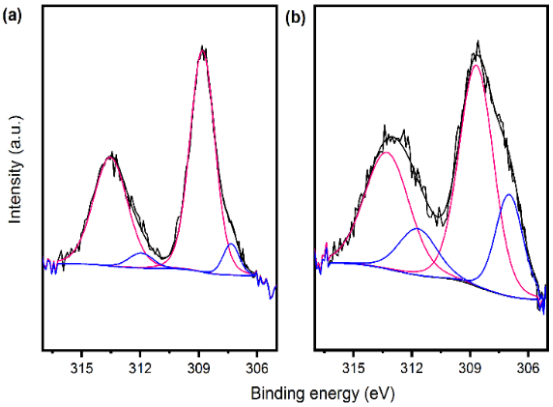

Fig. 4. Rh 3d XPS spectra of fresh (a) and used (b) Rh-1.3-In_2O_3 catalysts. Purple and blue lines show fitting of Rh^{3+} and reduced Rh species respectively.

408.9 eV between In^{3+} (406.4 eV) and expected peak position for In^0 (410.4) eV.[18] Such phenomenon has been noted as strong metal-support interaction (SMSI) between Rh and reducible supports such as TiO_2 and ZnO nanowires and plays an important role in stabilizing Rh atoms, which are prone towards sintering under the hydrogenation condition.[12,19]

The reducibility of Rh atoms was studied via H_2 temperature programmed reduction (TPR) experiments. Unpromoted In_2O_3 showed a small reduction feature at 160 °C attributed to creation of oxygen vacancies on the surface (Fig. 5).[4] Rh atoms in Rh-1.3-In_2O_3 catalysts were reduced at 95 °C. Tailing of this peak at higher temperature indicated partial reduction of In_2O_3 surface in the presence of Rh. The total hydrogen consumption in case of Rh-1.3-In_2O_3 was 0.067 mmol g^{-1}. Using CO pulse chemisorption, we calculated that 0.0068 mmol g^{-1} of Rh atoms in Rh-1.3-In_2O_3 were present on the surface assuming Rh single atom binds with two CO and In_2O_3 does not adsorb CO.[2] The theoretical consumption of H_2 to reduce Rh atoms on the surface is 0.0408 mmol g^{-1}. Therefore, the hydrogen consumption in TPR was 1.6 times higher than the expected value for complete reduction of Rh atoms. The excess hydrogen contributed towards formation of oxygen vacancy over the In_2O_3 surface.

The increase in abundance of oxygen vacancy was evident from the O 1s XPS spectra of catalysts (Fig. S9). The population of defective oxgyen in undoped In_2O_3 and fresh Rh-1.3-In_2O_3 was similar (38%) as Rh^{3+} replaced In^{3+} within the lattice. In the used catalyst, the relative abundance of defective oxygen species increased by 5% owing to the reduction of surface Rh^{3+} cations followed by the generation of oxygen vacancies over the In_2O_3 surface. This data suggests that incorporation of Rh increased the number of oxygen defects on the catalyst surface during the reaction. The oxygen vacancies were formed in less than 1 h after starting the reaction and remained stable as the reaction progressed. Analysis of Rh-1.3-In_2O_3 catalyst after 1 h of reaction (Fig. S10) showed that Rh was already reduced and the amount of defective oxygen was 43 %, which did not change after 5 h and 10 h of reaction.

The influence of oxygen defects on CO_2 adsorption was analyzed by desorption profile of adsorbed CO_2 from the catalyst surface. Temperature programmed desorption (TPD) spectra for CO_2 showed three peaks after CO_2 adsorption at room temperature (Fig. 6). Desorption at temperatures above 400 °C was due to CO_2 chemisorbed over the oxygen vacant sites.[10,20,21] Higher amount of chemisorbed CO_2 was present over Rh-1.3-In_2O_3 in comparison to In_2O_3. The desorption peak shifted from 405 °C for In_2O_3 to 440 °C for Rh-1.3-In_2O_3 owing to stronger chemisorption of CO_2. The stronger adsorption of CO_2 over fresh Rh-1.3-In_2O_3 suggests that the chemical environment of vacancies is different in the presence of Rh.

TPD spectrum after exposing the catalyst to conditions similar to reaction (300 °C, 0.1 MPa, CO_2:H_2 = 1:4) showed a prominent peak centered at 270 °C instead of the chemisorbed CO_2 (Fig. 6, red line). We postulate that this peak results from dehydrogenation of formate species formed on the surface during reaction. A similar CO_2 peak was observed during dehydrogenation of formic acid impregnated over Rh-1.3-In_2O_3 supporting the assertion (Fig. S11). Although, detection of intermediates by diffuse reflectance infrared Fourier transform spectroscopy (DRIFTS) was not successful owing to Drude absorption of IR beam over reduced In_2O_3 surface,[22] this study suggests that Rh single atom plays an crucial role as active site to strongly adsorb CO_2 and to convert it to formate, main intermediate for methanol production.[3]

In order to differentiate the activity of dispersed Rh from In_2O_3, we prepared a Rh-1.3-ZnO catalyst using the sol-gel method. Similar to Rh-1.3-In_2O_3, Rh was atomically dispersed in Rh-1.3-ZnO matrix (Fig. S12). Atomically dispersed Rh in ZnO showed high activity towards RWGS reaction whereas pure ZnO was not active (Fig. S13). It has been reported that atomically dispersed Rh can promote RWGS reaction via the formate pathway.[23,24] Therefore, we propose that, under reaction condition, in addition to generation of oxygen vacancies over the In_2O_3 surface, Rh also promotes strong CO_2 adsorption and its conversion to formate species, which are further hydrogenated to produce methanol in conjugation with neighbouring In atoms.

Density functional theory (DFT) calculations were used to investigate the localized molecular level structure of Rh doped within an In_2O_3 cluster and the activation of CO_2 on this site (See ESI). Rh preferred the most symmetric octahedral site with five O coordination having an average Rh-O bond length of 2.05 Å in the model, which was similar to value observed in EXAFS analysis. The incorporation of a Rh atom promoted removal of lattice oxygen around the Rh under hydrogenation condition, and the Rh atom was then stabilized by the interaction with neighbouring In atoms. Introduction of a CO_2 molecule onto the oxygen vacant Rh site caused activation of CO_2 by formation of

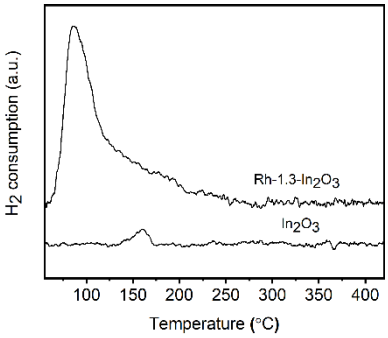

Fig. 5. H_2 TPR of In_2O_3 and Rh-1.3-In_2O_3 catalysts.

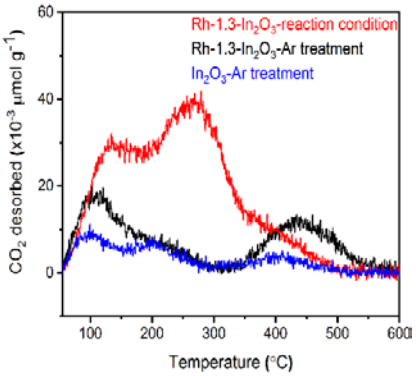

Fig. 6. Evolution of CO_2 during temperature programmed desorption after exposing the catalyst to CO_2 at room temperature or under reaction condition.

Rh–COO species. H_2 addition to the Rh centre produced a $Rh(H)_2(COO)$ structure, and one of the H atoms was transferred to activated CO_2, giving a formate specie with an activation energy of only 59 kJ mol^{-1} (Fig. S15). These results further support the activation of CO_2 at oxygen vacancies around Rh atoms and the intrinsic role of Rh for the CO_2 hydrogenation on Rh-In_2O_3 mixed oxide catalysts.

Conclusions

In conclusion, Rh was the most effective promotor among the group 8, 9 and 10 transition metals used for doping of In_2O_3 for CO_2 hydrogenation to methanol. Rh was atomically dispersed in the In_2O_3 matrix and remained stable under reaction condition through a charge transfer from partially reduced In_2O_3 to Rh atoms. Other than just increasing oxygen defects, Rh itself participated in CO_2 hydrogenation. Rh promoted stronger CO_2 adsorption around itself by modifying the chemical environment. Incorporation of Rh atom at the active site facilitates the formation of formate species, that are intermediate for methanol synthesis over In_2O_3. Thus, Rh plays an important role in CO_2 hydrogenation along with increasing H_2 dissociation and oxygen vacancy creation over In_2O_3. Rh loading of as low as 1.3 atom% (0.96 wt%) was sufficient to achieve high and stable STY of 1.0 g_{MeOH} h^{-1} g_{cat}^{-1} for methanol. High methanol STY achieved under industrially relevant condition in our study clearly shows the merit of atomically dispersed Rh in In_2O_3 catalysts. We believe that our study will give more insight in the development of atomically dispersed metal catalysts.

Conflicts of interest

There are no conflict of interests.

Acknowledgements

Part of this work was funded by Integrated Materials Creation Chemistry Research Promotion Organization, Japan. AMK and CT acknowledge the support by the American Chemical Society Petroleum Research Fund, award number PRF# 55575-ND5. Use of the Stanford Synchrotron Radiation Light Source (SSRL, beamlines 4-1 user proposal 5104), SLAC National Accelerator Laboratory is supported by the U.S. Department of Energy, office of Basic Energy Science under Contract No. DE-AC02-76SF00515.

Notes and references

1 J. Zhong, X. Yang, Z. Wu, B. Liang, Y. Huang and T. Zhang, Chem. Soc. Rev., 2020, **49**, 1385.
2 M. B. Fichtl, D. Schlereth, N. Jacobsen, I. Kasatkin, J. Schumann, M. Behrens, R. Schlögl and O. Hinrichsen, *Appl. Catal. A,* 2015, **502**, 262.
3 J. Ye C. Liu, D. Mei and Q. Ge, *ACS Catal.,* 2013, **3**, 1296.
4 O. Martin, A. J. Martín, C. Mondelli, S. Mitchell, T. F. Segawa, R. Hauert, C. Drouilly, D. Curulla-Ferré and J. Pérez-Ramírez, *Angew. Chem. Int. Ed.,* 2016, **55**, 6261.
5 Z. Shi, Q. Tan and D. Wu, *AIChE J.,* 2019, **65**, 1047–1058.
6 A. Bavykina, I. Yarulina, A. J. A. Abdulghani, L. Gevers, M. N. Hedhili, X. Miao, A. R. Galilea, A. Pustovarenko, A. Dikhtiarenko, A. Cadiau, A. A. Tapia, J. L. Hazemann, S. M. Kozlov, S. O. Chikh, L. Cavallo and J. Gascon, *ACS Catal.,* 2019, **9**, 6910.
7 J. Ye, C. J. Liu, D. Mei and Q. Ge, *J. Catal.,* 2014, **317**, 44.
8 N. Rui, Z. Wang, K. Sun, J. Ye, Q. Ge and C. J. Liu, *Appl. Catal. B,* 2017, **218**, 488.
9 J. L. Snider, V. Streibel, M. A. Hubert, T. S. Choksi, E. Valle, D. C. Upham, J. Schumann, M. S. Duyar, A. Gallo, F. Abild-Pedersen and T. F. Jaramillo, *ACS Catal.* 2019, **9**, 3399.
10 M. S. Frei, C. Mondelli, R. García-Muelas, K. S. Kley, B. Puértolas, N. López, O. V. Safonova, J. A. Stewart, D. Curulla Ferré and J. Pérez-Ramírez, *Nat. Commun.,* 2019, **10**, 3377.
11 M. M. Li, H. Zou, J. Zheng, T. Wu, T. Chan, Y. Soo, X. Wu, X. Gong, T. Chen, K. Roy, G. Held and S. C. E. Tsang, *Angew. Chem. Int. Ed.,* 2020, **59**, 2.
12 R. Lang, T. Li, D. Matsumura, S. Miao, Y. Ren, Y. T. Cui, Y. Tan, B. Qiao, L. Li, A. Wang, X. Wang and T. Zhang, *Angew. Chem. Int. Ed.,* 2016, **55**, 16054.
13 R. D. Shannon, *Acta Crystallogr. A,* 1976, **32**, 751.
14 D. B. Buchholz, Q. Ma, D. Alducin, A. Ponce, M. Jose-Yacaman, R. Khanal, J. E. Medvedeva and R. P. H. Chang, *Chem. Mater.,* 2014, **26**, 5401.
15 C. A. Hoel, J.-F. Gaillard and K. R. Poeppelmeier, *J. Solid State Chem.,* 2010, **183**, 761.
16 Y. Kwon, T. Y. Kim, G. Kwon, J. Yi and H. Lee, *J. Am. Chem. Soc.,* 2017, **139**, 17694.
17 A. Bueno-López, I. Such-Basáñez and C. S. D. Lecea, *J. Catal.,* 2006, **244,** 102.
18 J. F. Moluder, W. F. Stickle, P. E. Sobol and K. D. Bomben, *Handbook of X-ray Photoelectron Spectroscopy*, Perkin-Elmer Corporation, Minnesota, 1992.
19 M. K. Samantaray, V. D'Elia, E. Pump, L. Falivene, M. Harb, S. O. Chikh, L. Cavallo, J. M. Basset, *Chem. Rev.,* 2019, **120**, 734.
20 P. Gao, S. Li ,X. Bu, S. Dang, Z. Liu,H. Wang, L. Zhong, M. Qiu, C. Yang, J. Cai, W. Wei and Y. Sun, *Nat. Chem.,* 2017, **9**, 1019.
21 C. Chou and R. F. Lobo, *Appl. Catal. A,* 2019, **583**, 117144.
22 L. M. Reyes, PhD thesis, University of Toronto, 2017.
23 Q. Zhang, L. Guo, Z. Hao, *Polyhedron,* 2018, **146,** 108.
24 Z. Cao, L. Guo, N. Liu, X. Zheng, W. Li, Y. Shi, J. Guo and Y. Xi, *RSC Adv.,* 2016, **6**, 108270.s.